Practical considerations on the use of low RF-fields and cosine modulation in high-resolution NMR of I = 3/2 spin quadrupolar nuclei in solids

Akiko Sasaki, Julien Trebosc, Hiroki Nagashima, Jean-Paul Amoureux

Practical considerations on the use of low RF-fields and cosine modulation in high-resolution NMR of I = 3/2 spin quadrupolar nuclei in solids

Akiko Sasaki,[a,b] Julien Trébosc,[c] Hiroki Nagashima,[a] Jean-Paul Amoureux,[d,e,*]

[a] *Interdisciplinary Research Center for Catalytic Chemistry, National Institute of Advanced Industrial Science and Technology (AIST), 1-1-1 Higashi, Tsukuba, Ibaraki 305-8565, Japan.*

[b] *Bruker Japan K.K., 3-9, Moriya-cho, Kanagawa-ku, Yokohama-shi, Kanagawa 221-0022, Japan.*

[c] *Univ. Lille, CNRS, INRAE, Centrale Lille, Univ. Artois, FR 2638 - IMEC – Institut Michel-Eugène Chevreul, F-59000 Lille, France.*

[d] *Bruker Biospin, 34 rue de l'industrie, F-67166 Wissembourg, France.*

[e] *Univ. Lille, CNRS, Centrale Lille, ENSCL, Univ. Artois, UMR 8181 – UCCS – Unit of Catalysis and Chemistry of Solids, F-59000 Lille, France.*

Despite its ease in experimental set up, the low sensitivity of MQMAS experiments is often a limiting factor in many practical applications. This is mainly due to the large radiofrequency (RF) field requirement of the two short hard-pulses often used for the optimum MQ excitation and conversion steps. Very recently, two novel MQMAS experiments have been proposed for I = 3/2 nuclei, namely lp-MQMAS and coslp-MQMAS, enabling an efficient MQ excitation/conversion with a reduced RF requirement, by utilizing two long pulses lasting one rotor period each, with or without cosine modulation. In this study, we focus on the practical considerations of these new methods and discuss their pros and cons to elucidate their appropriate use under both moderate and fast spinning conditions. Using four I = 3/2 (^{87}Rb, ^{71}Ga, ^{35}Cl and ^{23}Na) nuclei at a moderate magnetic field (B_0 = 14.1 T), we show the superior use of these experiments, especially for samples with large C_Q values and/or low-gamma nuclei. Compared to all other existing sequences, the coslp-MQMAS method with initial WURST signal enhancement is the most robust, efficient and resolved high-resolution 2D method for spin 3/2 nuclei. Furthermore, using {^{23}Na}-^{1}H spin systems, we demonstrate the sensitivity advantage of the WURST coslp-MQ-HETCOR acquisition upon ^{1}H detection and fast MAS conditions.

I. Introduction

Nuclei with spin I > 1/2, are subject to quadrupolar interactions that cause an anisotropic broadening of the NMR resonances in solids. For half-integer spin quadrupolar nuclei (I = 3/2, 5/2, 7/2 and 9/2), this broadening is proportional to the magnitude of the quadrupolar interaction, which can be described with the $C_Q = e^2qQ$ value. All transitions are affected by the large quadrupolar interactions, except the one-quantum central-transition (1Q-CT), between the $\pm$ ½ energy levels, which is only broadened by the much smaller second-order quadrupolar contribution. However, Magic-Angle Spinning (MAS) does not fully refocus this residual anisotropic broadening, and hence to obtain isotropic spectra of half-integer quadrupolar nuclei, high-resolution two-dimensional (2D) methods, such as MQMAS (multiple-quantum MAS)[1] and STMAS (satellite-transition MAS),[2] are required. Owing to the ease in its experimental set up, MQMAS has been widely used as a routine method, whereas STMAS is technically more challenging due to the practical requirements such as the precise control of the spinning frequency and the accurate setting of the spinning axis to the magic angle.[3,4] Up to now, the low sensitivity of MQMAS, which originates from the use of 'forbidden' multiple-quantum coherences, is often a limiting factor in many practical applications. On the other hand, STMAS is more sensitive than MQMAS, but more challenging. Globally, MQMAS and STMAS are two complementary techniques, because the comparison of their isotropic dimensions allows to detect the presence of μs motions around the quadrupolar nucleus of interest.[5,6]

During the last decade, higher spinning rates have become more accessible on an everyday basis. Fast MAS experiments are highly promising in solid-state NMR investigations of half-integer spin quadrupolar nuclei, especially for samples with large C_Q sites or multiple sites with a considerable chemical shift difference. For example, we have recently reported such investigations on (i) MQMAS/STMAS detections of a large range of C_Q sites under moderate to fast MAS conditions,[7] and (ii) ^{1}H-detected MQ/ST-HETCOR (hetero-nuclear correlation) experiments, where the improved ^{1}H resolution under fast MAS was shown to be highly advantageous for the overall 2D sensitivity.[8,9]

In MQ-based experiments (i.e. MQMAS and MQ-HETCOR), the MQ excitation/conversion efficiency is presently limited, especially under fast MAS.[10] This is because for the optimum MQ excitation/conversion, the conventional hard-pulses require a large RF-field that depends on the C_Q values. Such large RFs are not always practically attainable for all nuclei, especially in the

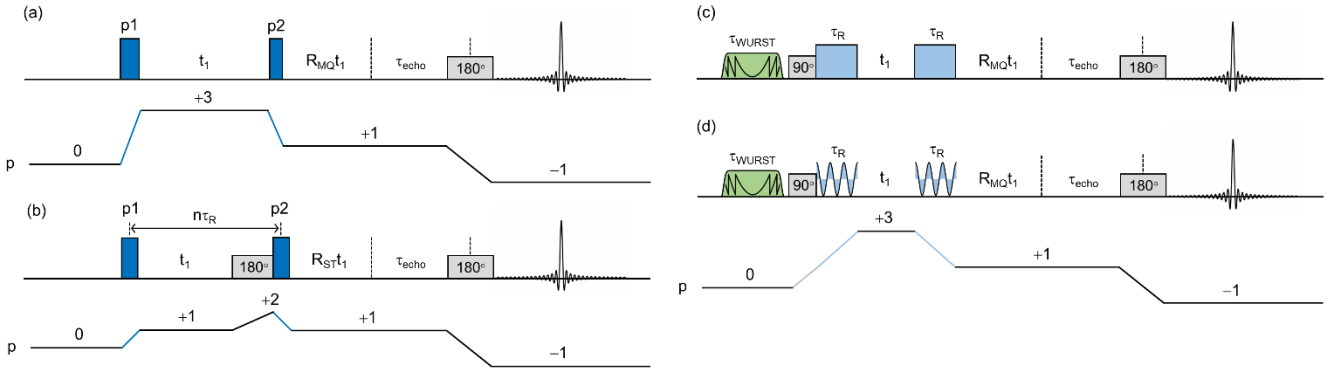

Fig.1. Pulse sequences and coherence transfer pathways used in this study for split-t_1 full-echo acquisition of (a) hp-MQMAS, (b) DQF-STMAS, (c) WURST lp-MQMAS and (d) WURST coslp-MQMAS experiments, where $\{R_{MQ}, R_{ST}\} = \{7/9, 8/9\}$ for I = 3/2 nuclei.

case of low-gamma nuclei, or when moderate or large diameter probes are used. In the following, this conventional sequence using two hard-pulses for the MQ excitation/conversion will be named hp-MQMAS. There exists a large variety of well-established experimental approaches to increase the sensitivity of MQMAS experiments (RIACT,[11] FAM,[12,13] DFS,[14] FASTER,[15] HS,[16] RAPT,[17] and CPMG-MQMAS[18]), although they often require a time-consuming optimization process of multiple parameters.

Very recently, Hung and Gan presented two novel variations for the MQ excitation/conversion pulses of I = 3/2 nuclei, namely lp-MQMAS (low-power or long-pulse MQMAS)[19] and coslp-MQMAS (cosine lp-MQMAS),[20] based on their previous lp-STMAS approach developed to excite the innermost STs with low RF requirement.[21] Both lp- and coslp-MQMAS sequences utilize two identical one rotor period (τ_R) pulses to transfer the magnetization between the 1Q-CT and the 3Q coherences. In lp-MQMAS, the one τ_R pulses are conventional rectangular ones, with the same offset frequency irradiating one satellite transition. In coslp-MQMAS, their magnitudes are cosine modulated, which is equivalent to a double frequency irradiation of the two satellite transitions.[20]

Both lp- and coslp-MQMAS experiments start with a 1Q-CT $\rightarrow$ 3Q transfer, and hence they benefit from any existing signal enhancement scheme for 1Q-CT signals, which can be applied prior to the first τ_R-pulse. Among them, the WURST (wideband, uniform rate, smooth truncation) pulse was chosen as the simplest one to set up.[19,20] It has been experimentally shown that the lp-MQMAS sequence results in a small amount of broadening along the isotropic dimension, which is the inevitable consequence of the application of long pulses on ST coherences.[20] It was consequently claimed that coslp-MQMAS is superior to lp-MQMAS because: (i) its isotropic linewidth is not broadened, and its efficiency is (ii) about 30% higher, and (iii) less dependent on the C_Q value.[20]

The lp- and coslp-MQMAS experiments have initially been developed under slow spinning, ν_R = 10-16 kHz.[19,20] Since then, one article showed up, in which the coslp-MQMAS approach was used to acquire ^{1}H/^{13}C/^{17}O 3D isotropic HETCOR spectra at B_0 = 18.8 T with ν_R = 90 kHz.[22] In these studies, the optimum conditions for the lp- and coslp-MQMAS variables were mostly reported as 'experimentally optimized' on the given sample.

In this study, we take a more general view and aim to establish the appropriate use and setup of these methods for potential applications in materials science. We focus on practical considerations of lp- and coslp-MQ-based experiments for I = 3/2 under moderate and fast MAS conditions, discussing the pros and cons of each approach. We also verify by both experiments and simulations, the versatility of the WURST sensitivity enhancement for the second-order broadened 1Q-CT lineshape. Additionally, we briefly compare the experimental setup of the z-filter and full-echo versions of WURST lp- and coslp-MQMAS experiments. Finally, we demonstrate the highly advantageous use of the WURST coslp-MQ-HETCOR approach over the ST-HETCOR counterpart, for the ease of experimental setup and the increased sensitivity, using {^{23}Na}-^{1}H systems (NaH_2PO_4 and Na_2HPO_4) at ν_R = 62.5 kHz.

II. Methods

All experiments were performed using a Bruker Avance NEO spectrometer with a B_0 = 14.1 T wide-bore magnet at a Larmor frequency of 196.37 (^{87}Rb), 183.06 (^{71}Ga), 58.81 (^{35}Cl) and 158.75 (^{23}Na) MHz, equipped with HX MAS probes using either ∅ = 3.2 mm rotors at ν_R = 16-20 kHz or ∅ = 1.3 mm at ν_R = 62.5 kHz. Maximum RF fields of ν_1 = 83 (^{87}Rb) and 42 (^{35}Cl) kHz were attained with ∅ = 3.2 mm, and ν_1 = 125 (^{87}Rb), 167 (^{71}Ga) and 137 (^{23}Na) kHz with ∅ = 1.3 mm. Powder samples ($RbNO_3$, Rb_2SO_4, β-Ga_2O_3, L-histidine.HCl.H_2O, NaH_2PO_4, Na_2HPO_4) were packed as purchased.

The MQMAS and STMAS pulse sequences used in this study are shown in Figs.**1** and **S1**, for split-t_1 full-echo and z-filter acquisition, respectively, and in Fig.**S2** for {I = 3/2}-^{1}H MQ/ST-HETCOR experiments. For the ease of data handling, most experiments were performed with the split-t_1 full-echo approach that does not require any extra shearing processing.[23] The recycling delays and echo-times for full-echo experiments (Fig.**1**) were {RD (s), τ_{echo} (ms)} = {0.5, 4} for Rb_2SO_4, {1.5, 0.2} for β-

Ga_2O_3, {1, 2.5} for L-histidine.HCl.H_2O, {0.25, 8} for $RbNO_3$ and {1, 6} for NaH_2PO_4 and Na_2HPO_4. The TopSpin pulse programs for WURST lp/coslp-MQMAS and -MQ-HETCOR experiments are provided in the Supplementary Information.

STMAS-based high-resolution experiments require a stringent technical set up, such as an accurate magic angle setting (e.g. 54.736 $\pm$ 0.002°) and a very stable spinning frequency (e.g. 1 part in 10^4), to acquire the isotropic spectra with little anisotropic bradening.[3,4] In this study, the magic angle was set on the sample of interest prior to the acquisition of STMAS and ST-HETCOR spectra, using the split-t_1 full-echo DQF-STMAS pulse sequences.[24] The spinning stability was maintained by a MAS III unit within $\pm$10 Hz at ν_R = 16, 20 or 62.5 kHz. Chemical shift scales, shown in ppm, were referenced using the sample of interest itself as a secondary reference, and all 2D spectra were referenced according to the unified representation.[25] Further experimental details are given in the figure captions.

All simulations were performed using the SIMPSON simulation programs.[26] The input variables were the magnetic field (B_0 = 14.1 T), the nucleus of interest, the spinning frequency (ν_R), the RF-field (ν_1) and the quadrupolar coupling constant (C_Q). The quadrupolar interaction with η_Q = 0 was taken into account up to the second-order, without scalar or dipolar coupling. To calculate the efficiency of the methods, coherences were selected to emulate the STMAS and MQMAS sequences without any delay, except for the rotor-synchronized STMAS experiment (t_{1min} = τ_R - p1/2 - p4 - p2/2). The efficiency was defined with respect to the signal observed after a CT-selective 90° pulse. For the WURST simulations, the sequence consisted of the WURST pulse followed by a CT-selective 90° pulse. The powder averaging parameters (i.e. crystal file and number of γ-angles) and the Δt maximum time step over which the Hamiltonian is considered time-independent were tested for convergence, and a combination of ZCW54 $\times$ 10 γ-angles,[27–29] with Δt = 0.1 μs was sufficient for the given range of C_Q values used in this study. Since both the real and imaginary parts of the signal were found to be significant, its magnitude ($\sqrt{(Re^2 + Im^2)}$) is plotted as the signal intensity. Further simulation details are given in the figure captions.

III. Results and discussion

We first briefly summarize a few essential points to remember upon practical consideration of lp- and coslp-MQMAS experiments, based on the theoretical treatment and experimental demonstrations given in the previous studies.[19–21] (i) For the MQ excitation/conversion, a one-rotor pulse creates an inversion between the 1Q-CT and 3Q coherences. (ii) The two identical one τ_R pulses need to be symmetrically applied for excitation and conversion to cancel the anisotropic dephasings related to long pulses.[19,20] (iii) In lp-MQMAS, the irradiation offset frequency of the τ_R-pulses, ν_{irr}, should be applied within the ST manifold, which means far off-resonance from the CT signal,[19] whereas in coslp-MQMAS, the τ_R cosine irradiation is applied near the CT signal, and ideally on the center-band position of the 1Q-STs.[20] (iv) The optimum RF requirement ($\nu_{1,opt}$) is higher by $\sqrt{2}$ in coslp- than lp-MQMAS, and is dependent on both the C_Q value and the spinning frequency (ν_R), namely, $\nu_{1,opt} \approx \sqrt{(C_Q\nu_R/12)}$ for lp-MQMAS and $\sqrt{(C_Q\nu_R/6)}$ for coslp-MQMAS.[20] (v) Spinning fluctuations may cause an additional line broadening and a t_1-noise along the isotropic dimension of lp-MQMAS, while coslp-MQMAS is robust to such spinning instabilities.[20] (vi) Both z-filter and full-echo acquisitions are plausible in lp- or coslp-MQMAS.[19] (vii) When the full-echo acquisition is employed, the phase modulation of the signal may cause confusion during the optimization process, but this problem can be circumvented by displaying the spectra in the magnitude mode.[19]

These practically important points to the successful acquisition of lp- and coslp-MQMAS signals are thoroughly illustrated in the following, using ^{87}Rb and ^{71}Ga having moderate and large C_Q sites respectively, and using ^{35}Cl (ν_0 = 58.81 MHz at 14.1 T) as a low-gamma nucleus, with the aid of both experiments and simulations. We should remind here that such isotropic 2D acquisition of half-integer quadrupolar nuclei may intrinsically take several hours or days. We have recently established the eligibility of Non-Uniform Sampling (NUS) schemes in MQMAS/STMAS and MQ/ST-HETCOR acquisitions, which can be conveniently employed to reduce the total experiment time of such long 2D experiments.[9] Where plausible, the applicability of 50% NUS acquisition in the indirect dimension is demonstrated, to reduce the total experiment time (T_{exp}) by a factor of 2.

III.1 ^{87}Rb of Rb_2SO_4 at ν_R = 20 and 62.5 kHz

In Fig.**2**, the ^{87}Rb isotropic projections of the STMAS and MQMAS high-resolution 2D spectra of Rb_2SO_4 are shown at ν_R = 20 and 62.5 kHz, with or without WURST enhancement for the MQMAS experiments using τ_R pulses. There are two rubidium species in this compound, Rb1 and Rb2, with (C_Q, η_Q) = (2.5 MHz, 0.9) and (5.3 MHz, 0.1), respectively.[30,31]

III.1.a WURST optimization

For spin 3/2 nuclei, the transfer of population related to the WURST pulse scales up by a factor of 2-3 the populations of the $\pm$1/2 Zeeman levels. As a result, the advantage of WURST coslp-MQMAS is apparent as its intensity is 1.5-2.0 times higher than that of STMAS for the same experimental time. Among the existing 1Q-CT signal enhancement schemes, the practical advantage of WURST is that its optimum conditions are robust with respect to its length (τ_{WURST}), its offset frequency (ν_{off}) and the RF field amplitude ($\nu_{1,WURST}$), and the WURST sweep range is set to the spinning frequency (i.e. $\nu_{sweep} = \nu_R$). This robustness is experimentally

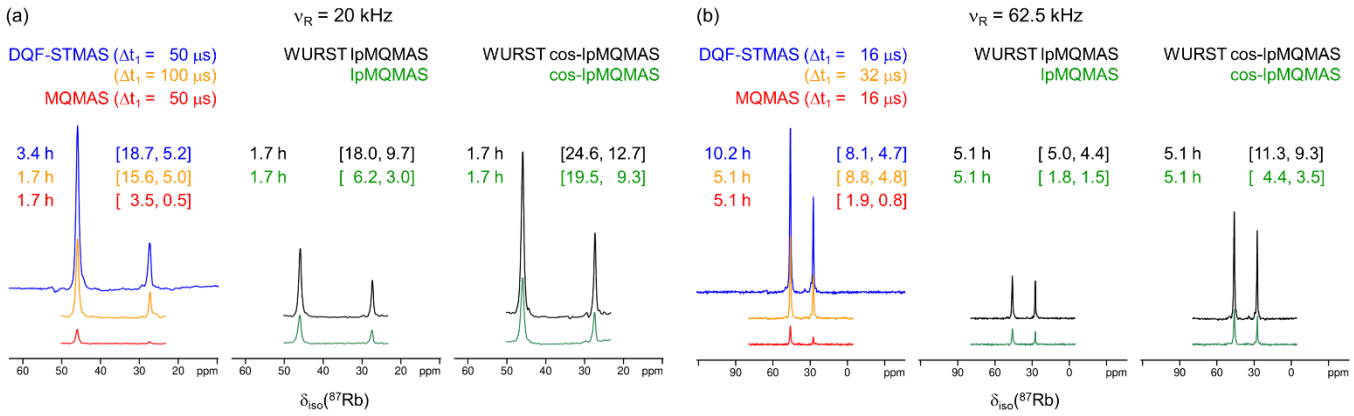

Fig.2. Isotropic projections of 2D ^{87}Rb DQF-STMAS, hp-, lp- and coslp-MQMAS full-echo spectra of Rb_2SO_4 at ν_R = 20 (a) and 62.5 (b) kHz, with or without the WURST enhancement for lp- and coslp-MQMAS. The T_{exp} values are indicated on the left sides and the Sensitivities (in $min^{-1/2}$) are given in the square brackets for the two Rb sites. NS = 192. WURST-80: $\nu_{1,WURST}$ = 19, ν_{off} = +200 kHz. lp-MQMAS: ν_1 = 45, ν_{irr} = +250 kHz. coslp-MQMAS: ν_1 = 75, ν_{irr} = +1, ν_{cos} = 250 kHz. (a) $\nu_{1,CT}$ = 10 kHz. hp-MQMAS & STMAS: ν_1 = 83 kHz; {p1, p2, p4} μs = {7.0, 2.0, 25} MQ, {2.5, 1.2, 25} ST. Δt_1{MQ, ST} = {50, 50/100} μs, N_{t1}{MQ, ST} = {64, 128/64}. At ν_R = 20 kHz, SW_{iso} is not large enough and hence the SNR and the Sensitivity values are only estimates. (b) $\nu_{1,CT}$ = 20 kHz. hp-MQMAS & STMAS: ν_1 = 125 kHz; {p1, p2, p4} μs = {3.0, 1.0, 12} MQ, {1.5, 0.6, 12} ST. Δt_1{MQ, ST} = {16, 16/32} μs, N_{t1}{MQ, ST} = {192, 384/192}.

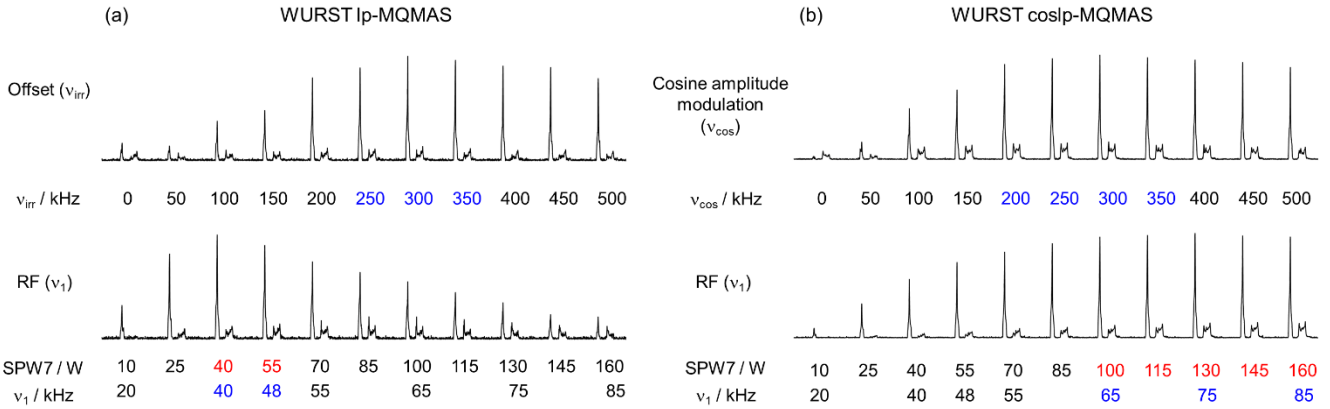

Fig.3. Experimental ^{87}Rb signal intensity profiles of WURST lp- and coslp-MQMAS variables of Rb_2SO_4 at ν_R = 20 kHz, with respect to the RF-field (ν_1) and the frequencies of either the irradiation (ν_{irr}) or the cosine modulation (ν_{cos}). NS = 48, T_{exp} = 24 s each. WURST-80: $\nu_{1,WURST}$ = 20, ν_{off} = +200 kHz.

demonstrated in Fig.**S3**, where a series of 1D ^{87}Rb full-echo WURST coslp-MQMAS spectra of Rb_2SO_4 is shown at ν_R = 20 and 62.5 kHz for a range of τ_{WURST}, ν_{off} and $\nu_{1,WURST}$ values. It must be noted the WURST optimization can be more easily obtained with a 90° CT-selective pulse, instead of the MQMAS here. The WURST signal intensity is on a plateau around the optimum conditions of each parameter (τ_{WURST} = 1-5 ms, ν_{off} = 200-500 kHz, and $\nu_{1,WURST}$ = 10-20 kHz). This experimental observation is verified by the simulations presented in Fig.**S4**. Except in Fig.**S3**, we have always used τ_{WURST} = 1 ms. Both our experiments and simulations confirm that WURST is efficient, robust and simple to set up for the 1Q-CT enhancement, which is a prerequisite to increase the sensitivity of subsequent lp- and coslp-MQMAS acquisition.

III.1.b lp- and coslp-MQMAS optimization

We then move on to illustrate the optimum conditions for the lp- and coslp-MQMAS variables of the τ_R-pulses: RF-field (ν_1) and frequency of either the rectangular pulses for lp-MQMAS (ν_{irr}), or the cosine modulations for coslp-MQMAS (ν_{cos}). We show in Fig.**3**, an experimental ^{87}Rb signal intensity profile of these parameters at ν_R = 20 kHz using Rb_2SO_4. As proposed in the previous studies, this optimization profile is shown in the magnitude mode.[19]

With coslp-MQMAS, the optimum RF field is higher than with lp-MQMAS ($\nu_{1,opt} \approx$ 75 and 40 kHz) and slightly more robust to RF inhomogeneity (second line in Fig.**3**).

For a given sample, the last parameter to be optimized is the frequency of either the irradiation, ν_{irr}, for lp-MQMAS or the cosine modulation, ν_{cos}, for coslp-MQMAS (first line in Fig.**3**). They both are on a plateau in the same range of $\nu_{irr} \approx \nu_{cos} \approx$ 200-350

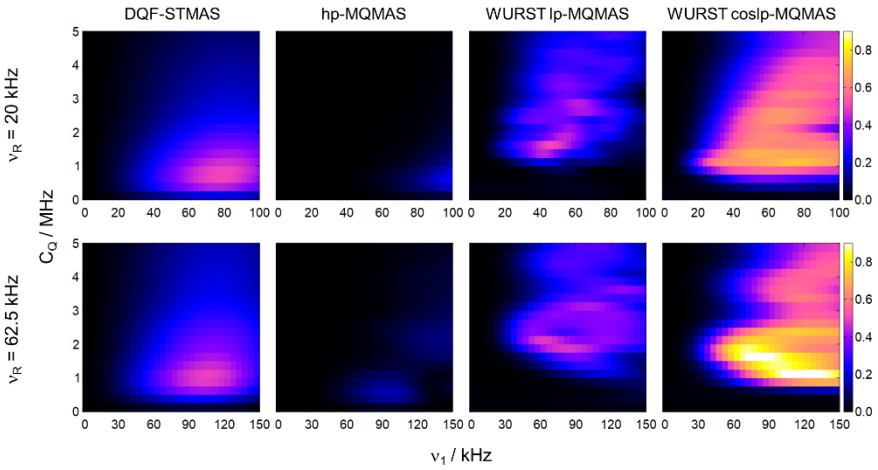

Fig.4. Simulated ^{87}Rb signal intensity of DQF-STMAS, hp-, WURST lp-and WURST coslp-MQMAS at ν_R = 20 and 62.5 kHz, with respect to C_Q and the RF-field (ν_1) of the MQ excitation and conversion pulses. For ν_R = 20/62.5 kHz, we have respectively observed: hp-MQMAS & STMAS, {p1, p2, p3, p4} μs = {6.0, 2.0, 12.5, 25} MQ, {1.6/1.2, 1.6/1.2, 12.5/6.25, 25/12.5} ST with $\nu_{1,CT}$ (p3, p4) = {10/20} kHz; WURST lp-MQMAS: ν_{irr} = +360/500 kHz; WURST coslp-MQMAS: ν_{cos} = 250/375 kHz. The intensity of WURST lp- and coslp-MQMAS was scaled up by a factor of 2.5 to take into account the WURST enhancement.

kHz, similar to that observed for the WURST pulse (Fig.**S4**). These experimental observations have been verified using the simulations shown in Fig.**S5**.

With the coslp-MQMAS sequence, it has been recommended to fix the carrier frequency (ν_{irr}) of the cosine modulation of the τ_R-pulses onto the center-band position of the 1Q-STs.[20] To verify this point, we show in Fig.**S6** the ^{87}Rb 1D spectra recorded at ν_R = 20 kHz with various ν_{irr} values and one observes that the sequence is robust with respect to this parameter. However, simulations (not shown) suggest that as C_Q increases, there is a decrease in signal as the pulse offset from the ST increases. This point has been confirmed with the optimization of the ^{71}Ga experiments (section III.2).

Having established the optimum conditions for the lp- and coslp-MQMAS variables, we can now safely compare the efficiency of such novel methods versus the conventional approaches. Fig.**4** summarizes the simulated ^{87}Rb signal intensity of STMAS and MQMAS spectra at ν_R = 20 and 62.5 kHz, with respect to C_Q and the RF-field (ν_1) of the MQ excitation and conversion pulses. In good agreement with the 2D experimental results (Fig.**2**), WURST coslp-MQMAS shows the highest sensitivity, especially for large C_Q values.

It should be noted here that, upon 2D rotor-synchronized acquisition ($\Delta t_1 = \tau_R$), ST-based experiments such as STMAS or ST-HETCOR take a twice-longer time than the analogous MQMAS or MQ-HETCOR to achieve the same resolution. This is because the isotropic spectral width (SW_{iso}) is twice larger in ST-based experiments than in their MQ-based counterparts. When the expected isotropic peaks lie within a narrow chemical shift range, an optimized rotor synchronization can be conveniently employed in ST-based experiments to reduce the total 2D experimental time, T_{exp},[9] by incrementing the t_1 value by a multiple of the rotor period and scaling down the spectral width. This has been illustrated in Fig.**2**, where the STMAS acquisition was performed with $\Delta t_1 = \tau_R$ and also $2\tau_R$, then reducing SW_{iso} and T_{exp} by a factor of 2, making it comparable to the MQMAS counterpart. The Sensitivity ($S = SNR/\sqrt{T_{exp}}$ in $min^{-1/2}$) of the 2D ^{87}Rb isotropic peaks is indicated in Fig.**2** for all variations. Our comparison of the Sensitivity values confirms that WURST coslp-MQMAS is indeed the method of choice for the best sensitivity and resolution for a given spectrometer time, without the need for the so-called STMAS specifications. As example, at ν_R = 62.5 kHz, for the two ^{87}Rb species we observe S = 8.8/4.8 and 11.3/9.3 $min^{-1/2}$ with STMAS and WURST coslp-MQMAS, respectively (Fig.**2**). Whatever the analyzed nucleus and the spinning frequency, we have always observed (i) a WURST gain of ca. 2.5, confirmed by the simulations shown in Figs.**S4** and **S7**, and a smaller (ii) sensitivity and (iii) isotropic resolution of the lp-MQMAS methods as compared to the coslp-MQMAS ones. Therefore, in the following figures of the main text, for the one τ_R based MQMAS methods we will only present the results recorded with WURST coslp-MQMAS.

III.2 ^{71}Ga of β-Ga_2O_3 (C_Q = 8.3, 11.0 MHz) at ν_R = 62.5 kHz

Having thoroughly established the experimental variables and hence the expected optimum conditions for the τ_R-based approaches using Rb_2SO_4, we now demonstrate that one of the main power of WURST coslp-MQMAS lies in the efficient detection of species with large C_Q values.

Ga_2O_3 samples have been employed in several solid-state ^{71}Ga NMR investigations, mostly under MAS,[32–37] and 2D WURST lp- and coslp-MQMAS spectra of β-Ga_2O_3 were demonstrated at very high magnetic fields (B_0 = 19.6-20.0 T) with ν_R = 14 kHz.[19,20] Our as-purchased Ga_2O_3 sample was found to be a pure β-Ga_2O_3 form with two Ga sites with (C_Q (MHz), η_Q) = (8.3, 0.1) and (11, 0.9).[32,34] In this study, we demonstrate the feasibility of acquiring high-resolution ^{71}Ga 2D spectra of such large C_Q sites with a moderate

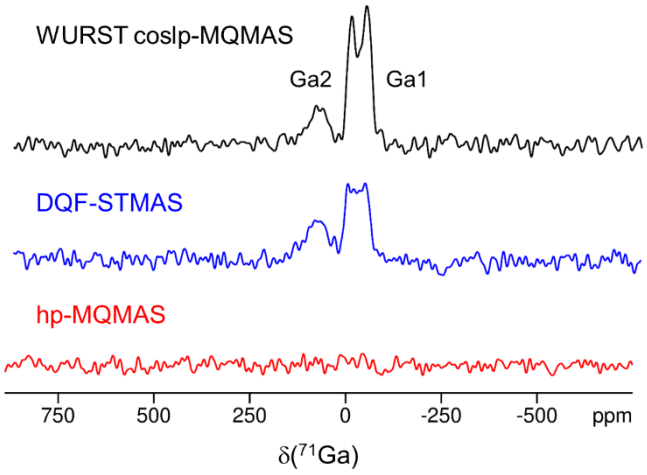

Fig.5. A comparison of 1D ($t_1 = 0$) ^{71}Ga DQF-STMAS, hp-MQMAS and WURST coslp-MQMAS spectra of β-Ga_2O_3 at ν_R = 62.5 kHz. NS = 384, T_{exp} = 9.5 min each. hp-MQMAS & DQF-STMAS: ν_1 = 167 & 20 kHz. {p1, p2, p4} μs = {3.0, 1.0, 12} MQ, {1.0, 0.6, 12} ST. WURST coslp-MQMAS: ν_1 = 143, ν_{irr} = +10, ν_{cos} = 300 kHz. WURST-80: $\nu_{1,WURST}$ = 25, ν_{off} = +500 kHz.

magnetic field (B_0 = 14.1 T), owing to the combination of fast spinning (ν_R = 62.5 kHz) and the aforementioned one τ_R based MQMAS approaches.

Fig.**5** shows a comparison of the 1D ($t_1 = 0$) STMAS and MQMAS ^{71}Ga spectra of β-Ga_2O_3 at ν_R = 62.5 kHz. As expected, the conventional hp-MQMAS fails for such large C_Q sites, while the WURST coslp-MQMAS signal intensity is higher than that of STMAS. In Fig.**S8a**, we compare the simulated ^{71}Ga signal intensity of STMAS and MQMAS methods with respect to C_Q and ν_1 of the excitation/conversion pulses. The poor sensitivity of hp-MQMAS is confirmed, except for small values of $C_Q \approx 1$ MHz. One also observes the sensitivity advantage of WURST coslp-MQMAS over STMAS, especially for large C_Q values.

This is also the case in Fig.**6a**, which compares the isotropic projections of ^{71}Ga 2D spectra of β-Ga_2O_3 at ν_R = 62.5 kHz. The WURST coslp-MQMAS signal intensity is similar to that of STMAS, without the stringent requirements e.g. the prior need for the accurate adjustment of the spinning axis to the magic angle.

We should note here that, in Fig.**6a**, the larger C_Q site (Ga2) should appear at 280 ppm in the isotropic dimension but that it is aliased and appears at about 100 ppm. For compounds with large chemical shift differences, increasing SW_{iso} may be helpful upon spectral interpretation. This can be achieved either by physically increasing ν_R or by decreasing the t_1 increment with MQMAS methods (e.g., Δt_1 = 8 instead of 16 μs at ν_R = 62.5 kHz), although the latter option inevitably increases T_{exp}. This loss in time can be compensated by the appropriate use of a Non-Uniform Sampling (NUS). We have previously demonstrated the simplicity and robustness of a $NUS_{bi\text{-}exp}$ method with simultaneous exponential decreasing sampling density and increasing sampling delay, and we have established that 32-50% NUS can be safely employed in the acquisition of isotropic spectra of half-integer quadrupolar nuclei.[9] As shown in Fig.**6b**, the identical isotropic information on Ga1 and Ga2 is obtained in only half of the time taken to record the conventional, non-NUS spectrum. We should emphasize here that $NUS_{bi\text{-}exp}$ acquisition is particularly useful under fast MAS (e.g. ν_R = 62.5 kHz), where an intrinsically large number of Δt_1 increments are required to achieve the expected resolution in the isotropic spectrum of half-integer quadrupolar nuclei.

III.3 ^{35}Cl of L-histidine.HCl.H_2O at ν_R = 20 kHz

L-histidine.HCl.H_2O has been widely employed in ^{35}Cl NMR investigations (e.g. MAS,[38,39] DNP-CPMAS,[40] CPMG[41]), and recent studies are mostly concerned with the demonstration of ^{1}H-^{35}Cl correlation approaches, such as *D*-HMQC,[42–46] *D*-RINEPT,[47] *D*-

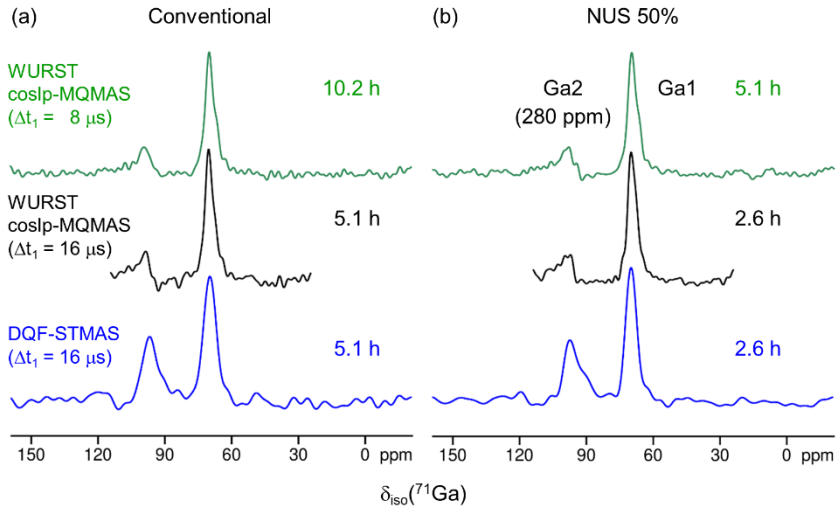

Fig.6. A comparison of isotropic projections of ^{71}Ga DQF-STMAS and WURST coslp-MQMAS spectra of β-Ga_2O_3 at ν_R = 62.5 kHz with (a) conventional and (b) 50% NUS acquisition. NS = 384, N_{t1} {MQ, ST}: (Conventional/NUS 50%) = {32/16, 64/32}. Further experimental details are given in Fig.5 caption.

RESPDOR,[48] and T-HMQC.[49,50] Despite its high natural abundance (75.8%), its low gyromagnetic ratio and hence Larmor frequency (58.81 MHz at 14.1 T) limit the accessible range of RF-field. With our ∅ = 3.2 mm MAS probe, a maximum RF-field of only 40 kHz was achievable. This hinders the acquisition of conventional hp-MQMAS signals, which requires a high RF-field for efficient MQ excitation/conversion. This is experimentally demonstrated in Fig.**7**, where we compare the 1D ^{35}Cl (C_Q = 1.8 MHz, η_Q = 0.66)[39] STMAS, hp-MQMAS and WURST coslp-MQMAS spectra of L-histidine.HCl.H_2O at ν_R = 20 kHz. While the conventional hp-MQMAS resulted in only noise, the WURST coslp-MQMAS signal was larger than that of STMAS. It should be reminded again that the WURST pulse gives an enhancement factor of 2-3 under optimum conditions (Fig.**S7b**).

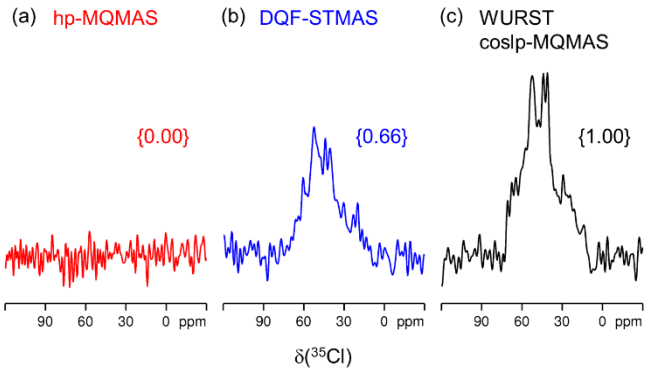

Fig.7. Comparison of 1D (t_1 = 0) ^{35}Cl (a) hp-MQMAS, (b) DQF-STMAS, and (c) WURST coslp-MQMAS spectra of L-histidine.HCl.H_2O at ν_R = 20 kHz. NS = 192, T_{exp} = 3.2 min each. hp-MQMAS & STMAS: ν_1 = 40 & 10 kHz. {p1, p2, p4} μs = {4.5, 4.5, 25} MQ, and {4.0, 2.0, 25} ST. WURST coslp-MQMAS: ν_1 = 40, ν_{irr} = +3, ν_{cos} = 250 kHz. WURST-80: $\nu_{1,WURST}$ = 20, ν_{off} = +300 kHz. The relative intensities with respect to WURST coslp-MQMAS are given in the curly brackets.

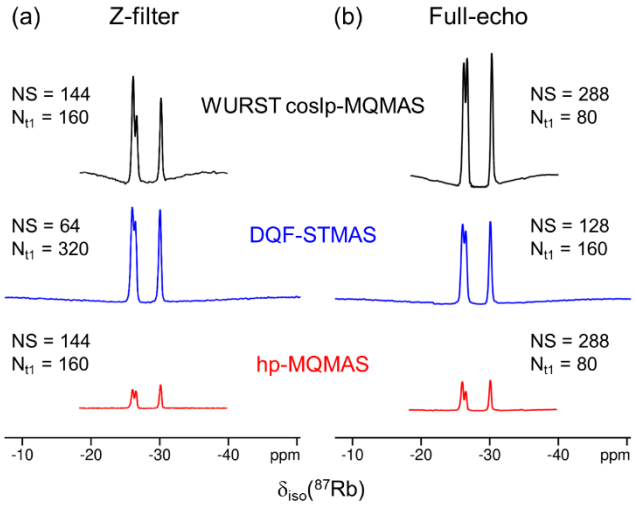

Fig.8. Isotropic projections of 2D ^{87}Rb DQF-STMAS, hp-MQMAS and WURST coslp-MQMAS spectra of $RbNO_3$ at ν_R = 16 kHz, with (a) z-filter and (b) full-echo acquisition. T_{exp} = 1.4-1.6 h each. Further experimental details are given in Fig.S10 caption.

It must be noted that in this case the WURST lp- and coslp-MQMAS sensitivities were similar (Fig.**S9**). This is because ν_1 was limited to 40 kHz with our 3.2 mm probe, whereas the simulations shown in Fig.**S8b** point out that with C_Q = 1.8 MHz, the optimum RF-fields are ca. 35 and 50 kHz for lp- and coslp-MQMAS, respectively. Moreover, one observes in Fig.**S9** that coslp-MQMAS leads to a narrower isotropic resonance (55 % 75 Hz) than lp-MQMAS. Last, as already demonstrated with β-Ga_2O_3 (Fig.**6**), 50% NUS can be safely employed for 2D isotropic acquisition, which doubles the sensitivity (Fig.**S9**).

III.4 ^{87}Rb of $RbNO_3$ at ν_R = 16 kHz

Since the one-rotor based MQMAS methods can be incorporated in both amplitude-modulated z-filter and phase-modulated full-echo pulse sequences,[19] one may envisage that, as with conventional hp-MQMAS, WURST coslp-MQMAS may be preferably employed with z-filter when the full-echo acquisition is not efficient, e.g. for materials that are either amorphous or with short T_2' values.

We have used ^{87}Rb NMR of $RbNO_3$ to analyse this point at ν_R = 16 kHz. There are three different Rb species in $RbNO_3$ with (C_Q (MHz), η_Q) = (1.7, 0.6), (1.7, 0.2) and (2.0, 0.9), called respectively Rb1, Rb2 and Rb3.[4] The 1D (t_1 = 0) spectra recorded with z-filter and full-echo acquisition of STMAS, hp-MQMAS, and WURST coslp-MQMAS are shown in Fig.**S10**, and in Fig.**8** we compare the corresponding isotropic projections of the 2D spectra. The STMAS and hp-MQMAS isotropic spectra are almost the same with z-filter and full-echo, whereas for WURST coslp-MQMAS, the full-echo signal is more sensitive than the STMAS counterpart, as expected, but the z-filter signal results in a decreased sensitivity. Furthermore, by considering the two left resonances (Rb2 and Rb3), we observe that STMAS is less resolved than WURST coslp-MQMAS, and it must be noted that these two peaks fully overlap with lp-MQMAS (not shown). These losses of resolution are related to spinning rate fluctuations and misadjusted magic angle.

We also realized that finding an optimum condition for the WURST coslp-MQMAS variables is more complicated for z-filter than for full-echo, due to the phase evolution. Indeed, when optimizing one particular parameter (ν_1, ν_{cos} or ν_{irr}), a local maximum in intensity is easily obtained. However, the absolute maximum without phase distortion was found to be dependent on the combination of these 3 variables, requiring the optimization process to be performed in multiple dimensions. Additionally, a set of chosen parameters with a good-looking 1D spectrum (i.e. no phase distortion) occasionally resulted in some artefacts in the 2D spectrum, while sometimes an 'unphasable' spectrum in 1D resulted in a better-looking 2D spectrum. Further investigations on this phase issue are currently ongoing.

III.5 {^{23}Na}-^{1}H NMR of NaH_2PO_4 and Na_2HPO_4 at ν_R = 62.5 kHz

In this last section, we demonstrate the advantageous use of the WURST coslp-MQMAS quadrupolar filter in the HETCOR experiments involving I = 3/2. Despite that HETCOR experiments between spin 1/2 nuclei have been routinely performed in solid-state NMR investigations, when a half-integer quadrupolar nucleus is correlated with another one, a structurally or chemically important information is often hindered by the quadrupolar broadening that causes a severe loss in resolution. This motivates the incorporation of a high-resolution MQMAS or STMAS quadrupolar filter in the HETCOR pulse sequences, leading to the development of MQ-HETCOR and ST-HETCOR experiments. Various population transfer schemes, to or from the half-integer quadrupolar nuclei, have been developed in the context of MQ/ST-HETCOR (e.g. MQ-CPMAS,[51–57] ST-CPMAS,[58] MQ-*J*-RINEPT,[57,59–62] and MQ-*D*-RINEPT[60,63–65]). The SPAM (Soft-Pulse Added-Mixing) sensitivity enhancement scheme[66–69] has also been implemented in MQ/ST-HETCOR pulse sequences (i.e. MQ/ST-SPAM-HETCOR). Recently, we have made a comparison of CPMAS, *D*-RINEPT and PRESTO transfers in MQ/ST-HETCOR schemes upon ^{1}H detection under fast MAS conditions.[8,9] Although CPMAS may be found efficient for relatively small C_Q sites, *D*-RINEPT should be generally recommended for a wider range of C_Q sites.

Very recently, the increased sensitivity of WURST coslp-MQMAS was shown to contribute to the successful acquisition of 3D isotropic ^{1}H/^{13}C/^{17}O (I = 5/2) HETCOR spectra at B_0 = 18.8 T and ν_R = 90 kHz.[22] In our present study, we focus on I = 3/2 nuclei and employ {^{23}Na}-^{1}H spin systems to demonstrate the feasibility of the WURST coslp-MQ-HETCOR 2D experiments and their preferential use for the ease of experimental setup and better sensitivity.

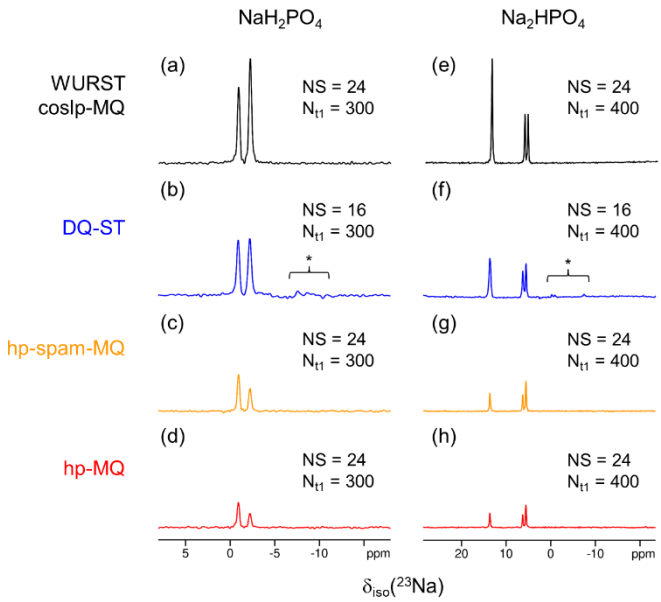

Fig.9. Comparison of isotropic projections of {^{23}Na}-^{1}H MQ/ST-HETCOR spectra of (a-d) NaH_2PO_4 and (e-h) Na_2HPO_4 at ν_R = 62.5 kHz, using the DQ-STMAS (b,f) or the hp- (d,h), hp-spam- (c,g) and WURST coslp-MQMAS (a,e) quadrupolar filters and a CPMAS transfer of magnetization. In ST-HETCOR spectra (b,f), the positions of artefacts are denoted by an asterisk (*). Δt_1{MQ, ST} μs = {64, 128} (a-d), {32, 64} (e-h), T_{exp} (h) = 0.7-1.0 (a-d), 1.8-2.7 (e-h). Further experimental details are given in Fig.S12 caption.

The MQ/ST-HETCOR pulse sequences used in this study are summarized in Fig.**S2**. We employed two Na salts, NaH_2PO_4 (C_Q = 1.6, 2.4 MHz) and Na_2HPO_4 (C_Q = 1.4, 2.3, 3.7 MHz).[70] As a prerequisite to HETCOR acquisition, we analyzed first the sensitivity of the quadrupolar filters under the fast MAS conditions required for ^{1}H detection. Indeed, during the last decade, following the development of fast spinning probes, ^{1}H detection has become frequently used owing to the increased ^{1}H resolution under fast MAS. In Fig.**S11** we compare the ^{23}Na isotropic projections of STMAS, hp-MQMAS and WURST coslp-MQMAS at ν_R = 62.5 kHz, with z-filter and full-echo acquisition. In consistence with the ^{87}Rb observations of $RbNO_3$ (Fig.**8**), the full-echo WURST coslp-MQMAS signals are more sensitive and resolved than the STMAS ones, but the z-filter signals resulted in a slight loss of sensitivity. It should be remembered here that, although two symmetrical pathways are simultaneously detected in MQ-HETCOR (like with z-filter MQMAS), the actual selected coherences are equivalent to the one used in the full-echo acquisition (See Figs.**1d**, **S1c** and **S2d**).

The ^{1}H and ^{23}Na 1D projections of {^{23}Na}-^{1}H MQ/ST-HETCOR spectra of NaH_2PO_4 and Na_2HPO_4 at ν_R = 62.5 kHz are shown in Figs.**S12** and **9**, respectively, using STMAS, hp-, hp-spam- and WURST coslp-MQMAS quadrupolar filters. In addition, in Fig.**S13**, we show the experimental WURST lp/coslp-MQ-HETCOR signal intensity profiles with respect to the three variables: ν_1, ν_{irr} and ν_{cos}. As observed in the context of MQMAS (Fig.**S11**), the WURST coslp-MQ-HETCOR quadrupolar filter is more sensitive than STMAS, and this is consequently reflected in the isotropic comparisons of {^{23}Na}-^{1}H MQ/ST-HETCOR spectra. Moreover, we have previously reported that, in ST-HETCOR spectra with I = 3/2, the presence of artefacts (denoted with asterisks (*) in the isotropic projection in Fig.**9**) is inevitable.[9] This is not the case with MQ-HETCOR spectra. Furthermore, despite the higher accessible RF-field with small rotors, the hp-MQMAS excitation/conversion efficiency is known to decrease at high spinning rates.[10] The WURST coslp-MQMAS approach does not suffer from this limitation, even at ultra-fast MAS that is necessary for the improved resolution upon ^{1}H detection in the direct dimension.

Although we have chosen these two Na-H model samples with small to moderate C_Q values (1.6-3.7 MHz) for the comparative demonstration of MQ/ST-HETCOR variants at B_0 = 14.1 T in a reasonable amount of spectrometer time, one may take advantage of the high sensitivity of WURST coslp-MQ-HETCOR and apply it to large C_Q samples. It must be noted that, even at high-spinning rates, the ^{1}H resolution can still be enhanced using homonuclear decoupling schemes.[71–73]

IV. Conclusions

Following the recent development of two new sequences with two one-rotor pulses for the efficient MQ excitation/conversion of I = 3/2, namely lp- and coslp-MQMAS, we have performed a thorough examination on their variables in the context of MQMAS and MQ-HETCOR experiments, with the aid of simulations and experiments at a moderate magnetic field (B_0 = 14.1 T).

We employed a range of nuclei and samples with either moderate C_Q values and Larmor frequencies ($^{87}RbNO_3$, $^{87}Rb_2SO_4$, $^{23}NaH_2PO_4$, and $^{23}Na_2HPO_4$), large C_Q values (β-$^{71}Ga_2O_3$), or low Larmor frequency (L-histidine.H^{35}Cl.H_2O), to show the feasibility of lp- and coslp-MQMAS-based experiments under both slow and fast MAS conditions (ν_R = 16/20-62.5 kHz).

In both lp- and coslp-MQMAS-based acquisitions, a 1Q-CT initial signal enhancement provides a gain of 2-3 in sensitivity. We have shown that the WURST scheme with $\nu_{sweep} = \nu_R$, is robust and easy to set up with respect to its three variables (i.e. τ_{WURST} = 1-5 ms, ν_{off} = 200-500 kHz and $\nu_{1,WURST}$ = 10-20 kHz).

For the best robustness, sensitivity and resolution, WURST coslp-MQMAS is the method of choice irrespective of the nuclei, the C_Q values or spinning frequencies. This sequence is easy to set up experimentally as it does not require any stringent STMAS specification (perfect magic-angle and stable spinning frequency) to keep the best resolution. To decrease the experimental time this sequence can be used with a bi-exponential NUS sampling and a CPMG recycling of the signal.

It should be remembered that the one-rotor pulses serve as inversion pulses between the 1Q-CT and 3Q coherences, and they are compatible with both z-filter and full-echo acquisition, like the conventional MQMAS experiment. However, in z-filter WURST coslp-MQMAS experiments, we observed several issues such as phase complexities, a slight loss of sensitivity and a presence of 2D artefacts. Further investigations on these problems need to be performed.

For I = 3/2 nuclei, there exist only two 1Q-STs and one 3Q coherences. For higher spin values, the presence of other 1Q-STs and 3Q coherences introduces further complexities to the theoretical treatment, as the 1Q-CT ↔ 3Q transfers become less confined, causing coherence leakage during the selective inversion of the inner STs, resulting in a lower efficiency for the MQ excitation/conversion.[19,20] At the time of writing, similar investigations to this study are under progress for I > 3/2 systems and will be reported elsewhere. We hope that our thorough investigations on each variable of WURST coslp-MQMAS and coslp-MQ-HETCOR will serve as a reference point to an efficient set up of these experiments and contribute to increase the number of such successful demonstrations of these experiments in materials science in the near future.

Conflicts of interest

There are no conflicts to declare.

Acknowledgements

The authors would like to thank Dr. Sebastian Wegner (Bruker BioSpin GmbH) for the help with the implementation of the pulse sequences on TopSpin software.

References

1. L. Frydman and J. S. Harwood. *J. Am. Chem. Soc.* 1995, **117**, 5367.
2. Z. Gan. *J. Am. Chem. Soc.* 2000, **122**, 3242.
3. C. Huguenard, F. Taulelle, B. Knott and Z. Gan. *J. Magn. Reson.* 2002, **156**, 131.
4. S. E. Ashbrook and S. Wimperis. *Prog. Nucl. Magn. Reson. Spectrosc.* 2004, **45**, 53.
5. S. E. Ashbrook, S. Antonijevic, A. J. Berry and S. Wimperis. *Chem. Phys. Lett.* 2002, **364**, 634.
6. S. Antonijevic, S. E. Ashbrook, S. Biedasek, R. I. Walton, S. Wimperis and H. Yang. *J. Am. Chem. Soc.* 2006, **128**, 8054.
7. A. Sasaki, Y. Tsutsumi and J. P. Amoureux. *Solid State Nucl. Magn. Reson.* 2020, **108**, 101668.
8. A. Sasaki, J. Trébosc and J.-P. Amoureux. *J. Magn. Reson.* 2021, **329**, 107028.
9. A. Sasaki, J. Trébosc and J.-P. Amoureux. *J. Magn. Reson.* 2021, **333**, 107093.
10. J. P. Amoureux, M. Pruski, D. P. Lang and C. Fernandez. *J. Magn. Reson.* 1998, **131**, 170.
11. G. Wu, D. Rovnyak and R. G. Griffin. *J. Am. Chem. Soc.* 1996, **118**, 9326.
12. P. K. Madhu, A. Goldbourt, L. Frydman and S. Vega. *Chem. Phys. Lett.* 1999, **307**, 41.
13. H. Colaux, D. M. Dawson and S. E. Ashbrook. *J. Phys. Chem. A* 2014, **118**, 6018.
14. A. P. M. Kentgens and R. Verhagen. *Chem. Phys. Lett.* 1999, **300**, 435.
15. T. Vosegaard, P. Florian, D. Massiot and P. J. Grandinetti. *J. Chem. Phys.* 2001, **114**, 4618.
16. R. Siegel, T. T. Nakashima and R. E. Wasylishen. *Chem. Phys. Lett.* 2005, **403**, 353.
17. Z. Yao, H. T. Kwak, D. Sakellariou, L. Emsley and P. J. Grandinetti. *Chem. Phys. Lett.* 2000, **327**, 85.
18. T. Vosegaard, F. H. Larsen, H. J. Jakobsen, P. D. Ellis and N. C. Nielsen. *J. Am. Chem. Soc.* 1997, **119**, 9055.
19. I. Hung and Z. Gan. *J. Magn. Reson.* 2021, **324**, 106913.
20. I. Hung and Z. Gan. *J. Magn. Reson.* 2021, **328**, 106994.

21. I. Hung and Z. Gan. *Phys. Chem. Chem. Phys.* 2020, **22**, 21119.
22. I. Hung, E. G. Keeler, W. Mao, P. L. Gor, R. G. Griffin and Z. Gan. *J. Phys. Chem. Lett.* 2022, **13**, 6549−6558.
23. S. P. Brown and S. Wimperis. *J. Magn. Reson.* 1997, **124**, 279.
24. H. T. Kwak and Z. Gan. *J. Magn. Reson.* 2003, **164**, 369.
25. J. P. Amoureux, C. Huguenard, F. Engelke and F. Taulelle. *Chem. Phys. Lett.* 2002, **356**, 497.
26. M. Bak, J. T. Rasmussen and N. C. Nielsen. *J. Magn. Reson.* 2000, **147**, 296.
27. S. K. Zaremba. *Ann. di Mat. Pura ed Appl.* 1966, **73**, 293.
28. H. Conroy. *J. Chem. Phys.* 1967, **47**, 5307.
29. V. B. Cheng, H. H. Suzukawa and M. Wolfsberg. *J. Chem. Phys.* 1973, **59**, 3992.
30. T. Vosegaard, J. Skibsted, H. Bildsøe and H. J. Jakobsen. *J. Magn. Reson. - Ser. A* 1996, **122**, 111.
31. H. T. Kwak, S. Prasad, T. Clark and P. J. Grandinetti. *J. Magn. Reson.* 2003, **160**, 107.
32. D. Massiot, I. Farnan, N. Gautier, D. Trumeau, A. Trokiner and J. P. Coutures. *Solid State Nucl. Magn. Reson.* 1995, **4**, 241.
33. D. Massiot, V. Montouillout, F. Fayon, P. Florian and C. Bessada. *Chem. Phys. Lett.* 1997, **272**, 295.
34. J. T. Ash and P. J. Grandinetti. *Magn. Reson. Chem.* 2006, **44**, 823.
35. L. A. O'Dell, S. L. P. Savin, A. V. Chadwick and M. E. Smith. *Appl. Magn. Reson.* 2007, **32**, 527.
36. I. Hung and Z. Gan. *Chem. Phys. Lett.* 2010, **496**, 162.
37. H. Y. Playford, A. C. Hannon, M. G. Tucker, D. M. Dawson, S. E. Ashbrook, R. J. Kastiban, J. Sloan and R. I. Walton. *J. Phys. Chem. C* 2014, **118**, 16188.
38. R. P. Chapman and D. L. Bryce. *Phys. Chem. Chem. Phys.* 2007, **9**, 6219.
39. M. K. Pandey, K. Hashi, S. Ohki, G. Nishijima, S. Matsumoto, T. Noguchi, K. Deguchi, A. Goto, T. Shimizu, H. Maeda, M. Takahashi, Y. Yanagisawa, T. Yamazaki, S. Iguchi, R. Tanaka, T. Nemoto, T. Miyamoto, H. Suematsu, K. Saito, T. Miki and Y. Nishiyama. *Anal. Sci.* 2016, **32**, 1339.
40. D. A. Hirsh, A. J. Rossini, L. Emsley and R. W. Schurko. *Phys. Chem. Chem. Phys.* 2016, **18**, 25893.
41. A. R. Altenhof, Z. Gan and R. W. Schurko. *J. Magn. Reson.* 2022, **337**, 107174.
42. M. K. Pandey, H. Kato, Y. Ishii and Y. Nishiyama. *Phys. Chem. Chem. Phys.* 2016, **18**, 6209.
43. A. Venkatesh, X. Luan, F. A. Perras, I. Hung, W. Huang and A. J. Rossini. *Phys. Chem. Chem. Phys.* 2020, **22**, 20815.
44. A. V. Wijesekara, A. Venkatesh, B. J. Lampkin, B. VanVeller, J. W. Lubach, K. Nagapudi, I. Hung, P. L. Gor'kov, Z. Gan and A. J. Rossini. *Chem. - A Eur. J.* 2020, **26**, 7881.
45. F. A. Perras, T. W. Goh and W. Huang. *Solid State Nucl. Magn. Reson.* 2022, **120**, 101807.
46. P. Raval, J. Trébosc, T. Pawlak, Y. Nishiyama, S. P. Brown and G. N. Manjunatha Reddy. *Solid State Nucl. Magn. Reson.* 2022, **120**, 101808.
47. A. Venkatesh, M. P. Hanrahan and A. J. Rossini. *Solid State Nucl. Magn. Reson.* 2017, **84**, 171.
48. B. A. Atterberry, S. L. Carnahan, Y. Chen, A. Venkatesh and A. J. Rossini. *J. Magn. Reson.* 2022, **336**, 107147.
49. I. Hung and Z. Gan. *J. Phys. Chem. Lett.* 2020, **11**, 4734.
50. R. Bayzou, J. Trébosc, I. Hung, Z. Gan, O. Lafon and J. P. Amoureux. *J. Chem. Phys.* 2022, **156**,.
51. S. H. Wang, S. M. De Paul and L. M. Bull. *J. Magn. Reson.* 1997, **125**, 364.
52. S. Steuernagel. *Solid State Nucl. Magn. Reson.* 1998, **11**, 197.
53. M. Roux, C. Marichal, J. L. Paillaud, C. Fernandez, C. Baerlocher and J. M. Chézeau. *J. Phys. Chem. B* 2001, **105**, 9083.
54. L. Delevoye, C. Fernandez, C. M. Morais, J. P. Amoureux, V. Montouillout and J. Rocha. *Solid State Nucl. Magn. Reson.* 2002, **22**, 501.
55. C. Fernandez, C. Morais, J. Rocha and M. Pruski. *Solid State Nucl. Magn. Reson.* 2002, **21**, 61.
56. A. Goldbourt, E. Vinogradov, G. Goobes and S. Vega. *J. Magn. Reson.* 2004, **169**, 342.
57. J. W. Wiench, G. Tricot, L. Delevoye, J. Trebosc, J. Frye, L. Montagne, J. P. Amoureux and M. Pruski. *Phys. Chem. Chem. Phys.* 2006, **8**, 144.
58. R. Siegel, J. Rocha and L. Mafra. *Chem. Phys. Lett.* 2009, **470**, 337.
59. J. W. Wiench and M. Pruski. *Solid State Nucl. Magn. Reson.* 2004, **26**, 51.
60. J. P. Amoureux, J. Trebosc, J. Wiench and M. Pruski. *J. Magn. Reson.* 2007, **184**, 1.
61. S. E. Ashbrook, M. Cutajar, C. J. Pickard, R. I. Walton and S. Wimperis. *Phys. Chem. Chem. Phys.* 2008, **10**, 5754.
62. M. Castro, V. R. Seymour, D. Carnevale, J. M. Griffin, S. E. Ashbrook, P. A. Wright, D. C. Apperley, J. E. Parker, S. P. Thompson, A. Fecant and N. Bats. *J. Phys. Chem. C* 2010, **114**, 12698.
63. C. Martineau, B. Bouchevreau, F. Taulelle, J. Trébosc, O. Lafon and J. Paul Amoureux. *Phys. Chem. Chem. Phys.* 2012, **14**, 7112.
64. B. Bouchevreau, C. Martineau, C. Mellot-Draznieks, A. Tuel, M. R. Suchomel, J. Trébosc, O. Lafon, J. P. Amoureux and F. Taulelle. *Chem. Mater.* 2013, **25**, 2227.
65. B. Bouchevreau, C. Martineau, C. Mellot-Draznieks, A. Tuel, M. R. Suchomel, J. Trebosc, O. Lafon, J. P. Amoureux and F. Taulelle. *Chem. - A Eur. J.* 2013, **19**, 5009.
66. Z. Gan and H. T. Kwak. *J. Magn. Reson.* 2004, **168**, 346.
67. J. P. Amoureux, L. Delevoye, S. Steuernagel, Z. Gan, S. Ganapathy and L. Montagne. *J. Magn. Reson.* 2005, **172**, 268.
68. J. P. Amoureux, L. Delevoye, G. Fink, F. Taulelle, A. Flambard and L. Montagne. *J. Magn. Reson.* 2005, **175**, 285.

69. J. P. Amoureux, A. Flambard, L. Delevoye and L. Montagne. *Chem. Commun.* 2005, 3472.
70. J. Trébosc, O. Lafon, B. Hu and J. P. Amoureux. *Chem. Phys. Lett.* 2010, **496**, 201.
71. M. Leskes, S. Steuernagel, D. Schneider, P. K. Madhu and S. Vega. *Chem. Phys. Lett.* 2008, **466**, 95.
72. Y. Nishiyama, X. Lu, J. Trébosc, O. Lafon, Z. Gan, P. K. Madhu and J. P. Amoureux. *J. Magn. Reson.* 2012, **214**, 151.
73. J. Tognetti, W. T. Franks, J. R. Lewandowski and S. P. Brown. *Phys. Chem. Chem. Phys.* 2022, **24**, 20258.